Luminosity Monitors and Their Applications for Detecting Target Boiling and Beam Fluctuations for Use in Parity Violation Experiments at Jefferson Lab

J. Hippert

William & Mary

Advisors: Prof. J.M. Finn (W&M) and R. Suleiman (MIT)

May 5, 2003

Abstract

The primary focus of this paper is a presentation of basic background information regarding parity violating experiments and then a discussion of the prominence of luminosity detectors in the Happex II experiment in Hall A of the Jefferson Lab Particle Accelerator. The goal of Happex II is to determine, with greater accuracy and certainty, any contribution to scattering asymmetries from strange quark anti-quark pairs in the sea quarks of protons. The luminosity monitors, "Lumis" for short, essentially consist of rectangular blocks of lucite connected to photomultiplier tubes. We have been using the Lumis to determine critical information about the electron beam line and, most importantly, the targets through which the beam line is being passed. Because the lumis have been set up at small deflection angles, relative to the target and beam line, where the sampling rate is 10-100 times greater than that in the vicinity of the two main spectrometers, they can quickly detect beam fluctuations between beam helicity states and also density fluctuations in the actual targets, 10-100 times faster than possible with the standard experimental setup. Both of these characteristics make lumis useful because it is much better to know how beam and target characteristics in a manner of days as opposed to weeks or months, especially when the experiment is only allocated a month of beam time. Some of the raw data and analysis from our preliminary tests was available last semester, but now the final results are available and we have concluded that we must minimize the effects of target boiling by implementing the new "race track" targets or possibly experimenting with the targets from HAPPEX I. It is also conceivable that we might be able to solve our problems by increasing the sampling frequency and using the lumi monitors to normalize away target density fluctuations.

1 Introduction

As we delve deeper and deeper into our understanding of the composition of matter, there is always the question, "what is it composed of?" We learned that matter is composed of atoms, that atoms are composed of protons, electrons, and neutrons, and that the protons and neutrons are in turn composed of quarks. We now have a model of the nucleon consisting of protons and neutrons which are composed of up and down quarks. Holding these quarks together are what we have come to call gluons. The current model of nucleon structure, thanks in large part to Dirac, Pauli, and Sachs, *et al.*, is defined in terms of various electric and magnetic form factors [9]. The goal of our experiment, HAPPEXII E99-115, is to revise and improve upon the current model by adding form factors resulting from strange quark anti-quark pairs. Though at this moment in time this is an endeavor to know for the sake of knowing, the physics uncovered here could one day have a great impact on science and humanity. After all, when the electron was first discovered, no one dreamed it would one day power all the niceties we have come to depend on in our lives. Thus we now set out to challenge the "Standard Model."

2 Jefferson Lab

Jefferson Lab, located in Newport News, is a cutting edge nuclear physics research facility for probing the quark structure of nuclei using electron scattering. Funded by the Department of Energy and other public sources, Jefferson Lab is currently the location of several state of the art experiments using parity violation to test the fundamental features of the standard model for nuclear physics. Essential to this effort is the 6 GeV super-conducting electron accelerator which provides unparalleled stability and beam control. A gigawatt of continuous power is available in a beam no larger than a human hair and the beam line is fitted with a switch yard to send the beam to any or all of three separate target areas (Halls A, B and C) (see Figure 1). There is even an upgrade to 12 GeV planned for the next decade. My primary focus has been the luminosity monitors which are being tested in Hall A for HAPPEX II [4], but which will also be installed in Hall C for use during the G_0 Experiment [6].

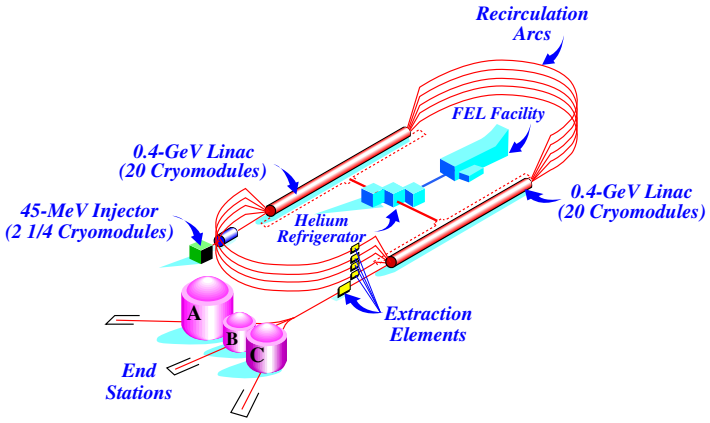

Figure 1: Jefferson Lab Schematic.

3 Parity Violation

Figure 2 demonstrates the basic concept of parity which is a discrete symmetry of the Electro-Magnetic (EM) interaction. Until the 1960's, when C. S. Wu *et al.* [1] studied the decay of Cobalt 60, it was believed to be a fundamental symmetry of nature. If you take the reflection of a process and it does not yield the same result as the original process, then parity is violated. This is the case for weak interactions (see Figure 4) between particles and is an important point to note in the experiment we are performing. Because the parity violating asymmetry is unique to the Weak Interaction, EM scattering will not contribute to the asymmetry, since it conserves parity. Also worth noting is the fact that the two figures on the "image" side of the mirror are equivalent if rotation is a good symmetry of nature. Therefore you can simply switch the electron polarization instead of having to switch the electron's momentum direction. This process is known as the switching of helicity.

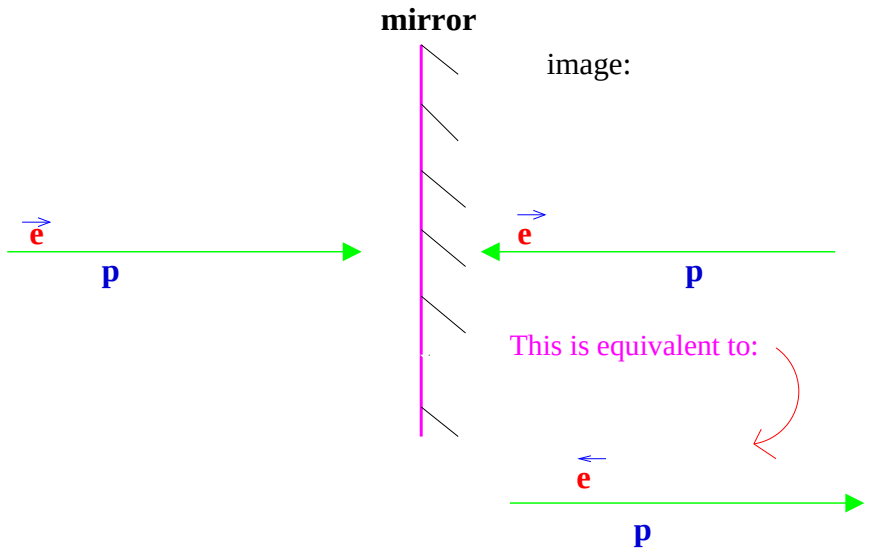

Figure 2: Parity Diagram: Shown here is the mirror reflection of the electron beam line. As you can see, the reflection changes the direction of the momentum vector, but not that of the axial spin vector.

3.1 Helicity

Helicity describes the momentum and spin of particles. When the momentum, p, and spin, s, are in the same direction, the helicity is right handed (see Figure 3). When they are in opposite directions, the helicity is left handed. For our purposes, switching helicity simply requires flipping the longitudinal polarization of the electron beam. If you refer to Figure 2, you will see that the two illustrations in Figure 3 are effectively the mirror images of each other.

3.2 Parity Requirements

The parity violating asymmetry can be defined as:

$$A = \frac{\sigma(R) - \sigma(L)}{\sigma(R) + \sigma(L)}$$

where σ is the cross section and is defined by [3]

$$\sigma \sim ([M^{\gamma} + M^{Z}]^2)$$

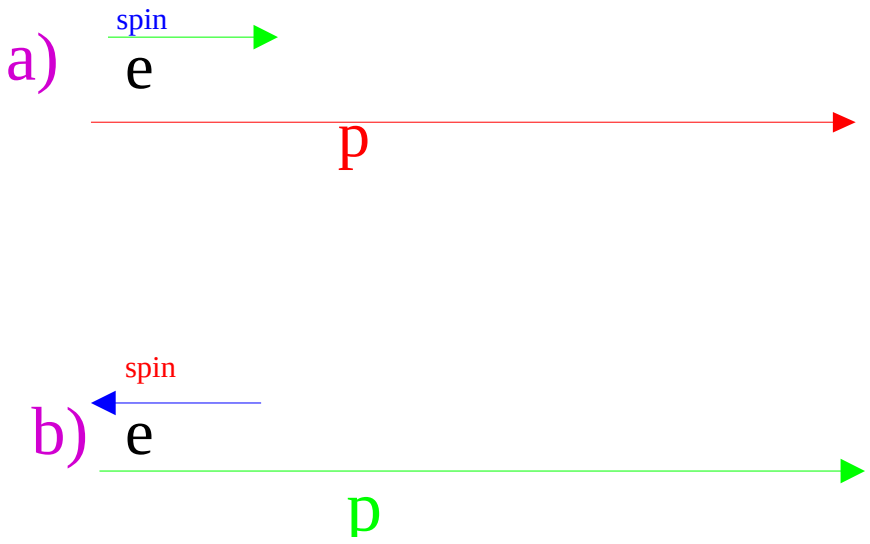

Figure 3: Helicity Illustration: If you switch the helicity in a), you get b), which is identical to a mirror reflection followed by a 180 degree rotation of the system.

and $\sigma(R)$ and $\sigma(L)$ refer to the right and left handed electron cross sections, respectively. M^{γ} is the amplitude of scattering for the photon interaction and M^{z} is the amplitude for the Weak Interaction coupling.

In a PV experiment, one measures the asymmetry for a helicity pair by measuring the difference divided by the sum of detected counts in the sample,

$$A_{measured} = \frac{N_R - N_L}{N_R + N_L}$$

The number of counts N_i in a detector is related to the luminosity L, the differential cross section $\frac{d\sigma}{d\Omega}$, and the detector acceptance $\Delta\Omega$ by

$$N = Lt_s \frac{d\sigma}{d\Omega}\Delta\Omega$$

where t_s is the sampling time. Luminosity, L, is proportional to the product of target thickness, T, and beam current, I, and is normally expressed in units of particles /sec/cm^2. A more correct expression for A is given by normalizing the measured counts to the instantaneous luminosity:

$$A_{corected} = \frac{N_R/L_R - N_L/L_L}{N_R/L_R + N_L/L_L}$$

Usually, one assumes that the target thickness is a constant over the sampling time and one normalizes the counting rate only for the current.

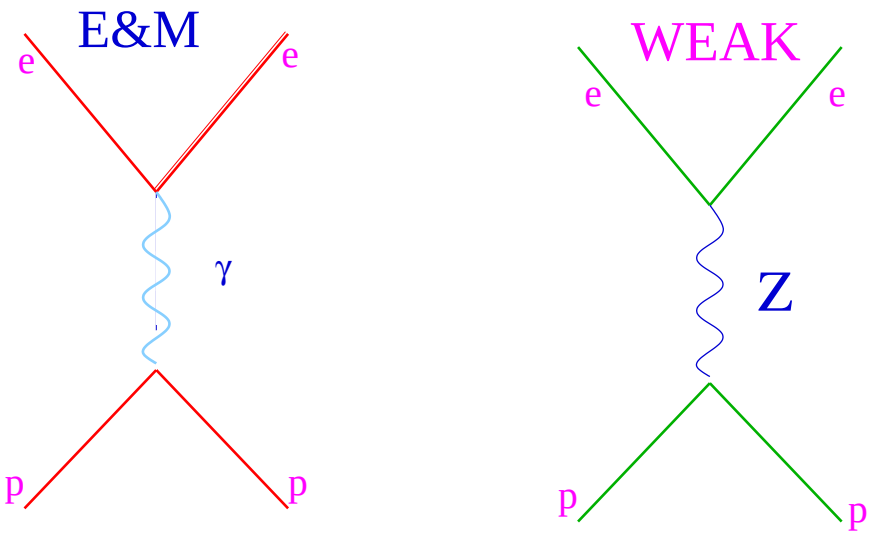

Figure 4: EM vs Weak Interaction: Parity is conserved for EM amplitude,M^{γ}, but not for the Weak amplitude M^{z}.

Because the parity violating asymmetry is small (ppm), there are certain things that must be carefully controlled. Most importantly is the possibility that there could be "false" asymmetries associated with helicity correlated beam or target fluctuations. When we say "asymmetry", we simply mean the uneven scattering of electrons from the target of protons (see Figure 5).

The best way to deal with the chance of beam asymmetry is to switch the helicity faster than the characteristic response time of the magnetic dipoles used to steer the beam. Then any beam effects will cancel each other out to a good approximation. With this in mind helicity is to be switched every 33 ms (30Hz). This means we should get 15 helicity pulse pairs every second. Furthermore, successive pulse pairs are chosen in a pseudo random fashion, again helping to assure cancellation.

Now, the asymmetries we hope to measure are very small. In fact, we anticipate them to be on the order of a few parts per million (ppm). Because of this, it is crucial that we are aware of any deviations in the electron beam and the target through which the beam pass so that we can adjust our raw data accordingly or make alterations to eliminate any fluctuations and, in doing so, obtain conclusive results as to whether there is a contribution to the detected asymmetry from strange quark anti-quark pairs.

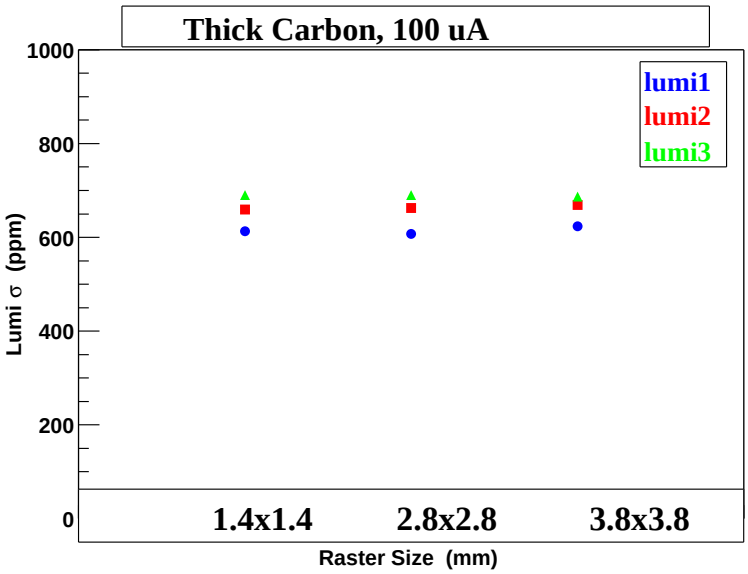

Figure 5: Lumi Sigma vs. Raster Size

Our main concern is that there may be a certain amount of asymmetry inherent in the beam and/or target. For low values of electron scattering angle, *theta*, the parity violating asymmetry should essentially be zero. In fact, at $\theta = 0$, the asymmetry must be identically zero, because there is no preferred axis! It is therefore possible to check your experimental system before running the entire experiment by simply checking to see if there is a measurable asymmetry for very small angles around $\theta = 0$ using the Lumi monitors. Moreover, the counting rate becomes enormous for small scattering angles, with a characteristic $1/\theta^4$ behavior. In just a few hours of beam time, it is possible to get a sensitive false asymmetry measurement due to the high flux of particles at low deflection angles where at higher deflection angles it would take weeks or months. This procedure is essential in ensuring you do not waste a month acquiring data which is tainted by error.

Finally, a feedback system is utilized. Initially, raw data is taken, and the raw beam current asymmetry is on the order of 1,000 ppm. A feedback loop is used to get this error down to about 1 ppm. At this point, we again measure and then correct for any residual effect, which is 1,000 times smaller thanks to the feedback (at the ppm level).

4 Experimental Statstics

To properly understand why target boiling is such a detriment to the HAPPEX II experiment, it is necessary to look at the statistical basis for concern. The statistical error of the experiment is given by

$$\delta_s = \sigma_s/\sqrt{N}$$

where σ_s is the error of a sample and N is the number of samples. Additional sources of error add in quadrature as

$$\delta_{tot} = \sqrt{(\sigma_s^2 + \sigma_b^2)}/\sqrt{N}$$

Typically, the major source of additional error is fluctuation due to target boiling. In HAPPEX I, the statistical error, σ_s, was much larger than σ_b. This means that over the course of the HAPPEX I experiment, δ_{tot} was essentially dominated by σ_s. Now, however, $(\sigma_s)^{HAPPEXII} << (\sigma_s)^{HAPPEXI}$ and the error associated with boiling, σ_b, has become relatively more significant. Since the sampling time is fixed, the number of samples is proportional to the running time. For each sample, $\sigma_s = (Rt_s)^{-1/2}$ where R is the rate of events and t_s is the sampling time. Since R is proportional to the current, I, of the beam, σ_s is proportional to $1/\sqrt{I}$, but σ_b, on the other hand, increases with the current, I, so that when current is increased, σ_b can become large with respect to σ_s. At some point, the increase of σ_b dominates and this becomes the limiting experimental factor. Let us look at two case studies:

- If we suppose that σ_b is one-third of σ_s, then over the course of an experiment we find $\delta_s = \sqrt{1.1}\sigma_s \sim 1.05\sigma_s/\sqrt{N}$. In this case the error is increased by 5%. To obtain the required experimental error one would get in the absence of σ_b, the runtime would have to be increased by 10%.
- In the second case where $\sigma_b \sim \sigma_s$, then $\delta\sigma = \sqrt{2}\sigma_s/\sqrt{N} \sim 1.4\sigma_s/\sqrt{N}$. Here, we see that the error is increased by 40%, and the run time would be effectively doubled if one wanted to achieve the same accuracy as would be possible in the absence of boiling. This second case is obviously unacceptable.

The reason that luminosity detectors are so advantageous is that at the small angles they were placed at relative to the beamline, the rate, R, is much higher. This makes studying

the target boiling much simpler and quicker becasue the high rate drastically lowers σ_s, and this makes the boiling much more apparent. This can be seen in Figure 6. In this figure a solid carbon target was used and you can see that, in the absence of boiling, the error in σ_s follows the expected $1/\sqrt{I}$ statistical behavior.

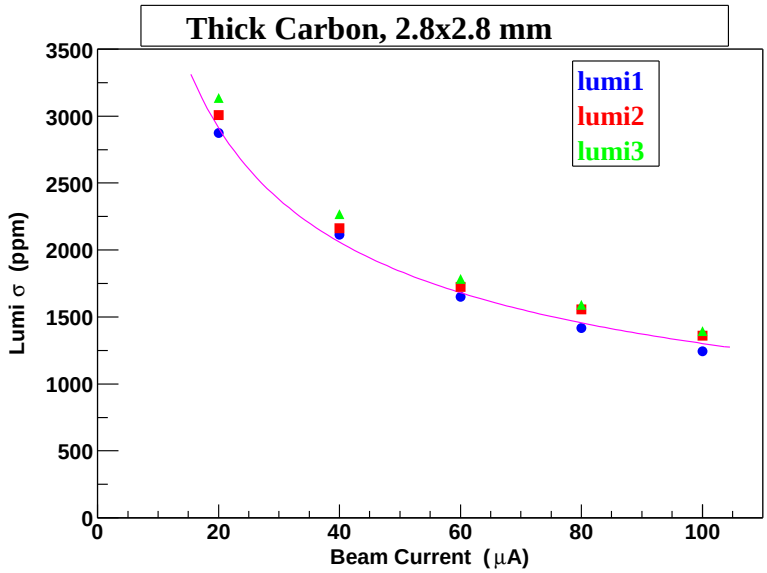

Figure 6: Lumi Sigma vs. Beam Current

5 Luminosity Detectors

5.0.1 How do the Lumis Work?

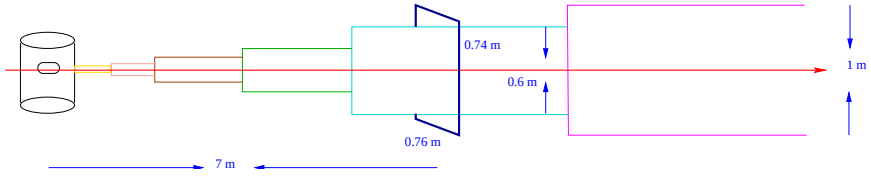

Figure 7: Lumi Diagram1: Here you can see the Lumi placement relative to the target and beamline in Hall A.

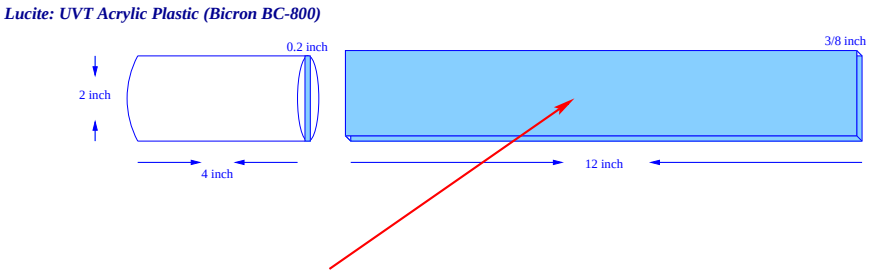

Figure 8: Lumi Diagram: This figure shows the lucite slab and photomultiplier tube that make up the "Lumi" apparatus.

The Lumis, surprisingly, are actually fairly simple devices (See Figures 7 and 8). They consist, in totality, of lucite bars, mounted normal to the beam line, which are attached to photo-multiplier tubes (PMTs). Particles entering the lucite emit visible Cherenkov light. This light arriving at the face of the PMT results in photoelectron knockout at the cathode surface. The electron signal is amplified in the photo-multiplier dynode chain, and the resulting current is then converted by Analog Digital Converters (ADCs) and processed in the counting house. The velocity gain of electrons in the dynode chain creates a sort of chain reaction as electrons travel through the tube dislodging more electrons ,which, in turn, dislodge other electrons resulting in a signal thousands of times stronger than that which originated at the photo-multiplier cathode.

5.0.2 Why Use Luminosity monitors?

Two important advantages to using Lumi detectors are that 1) they quickly determine any beam line fluctuations and 2) they also can detect density fluctuations within the LH2 and LD2 targets. Crucial to both these properties is that the luminosity monitors can be mounted at small scattering angles. In our tests, three sets of Lumis were placed at about 3.2 degrees, whereas the spectrometers are at about 6 degrees. The resulting flux differential is about a factor of 10. In the future, the Lumis will be placed at 0.5 degrees which will yield about a factor of 100 increase in flux. All this is made possible by their simple, compact design. The rather monolithic spectrometers can't be set nearly as close to the actual beam line due to their large footprint on the floor. Four Lumi monitors are placed in a symmetric position about the beam line to reduce systematic errors..

When we say that the Lumis can quickly see beam line fluctuations, we simply mean that they can determine fluctuations of the beam between helicities. As mentioned above, at a scattering angle of zero, the asymmetry resulting from the weak interaction, and therefore the asymmetry in general, is necessarily zero. It can therefore be inferred that any asymmetry that is measured by the Lumis, at least once they are set at 0.5 degrees, is actually an asymmetry due to beam differences relative to helicity. By determining the magnitude of these beam fluctuations early on, we are able to either account for them when making our calculations, or to simply fix the problem before we start the experiment. Either way, we will have our information 100 times faster when the experiment begins its commissioning studies.

As for the targets, by looking at the standard deviation, σ, and plotting it against the beam current, boiling can be determined. In theory, without boiling, the standard deviation should go down as the current goes up, simply because there should be more scattering events. If, however, the targets are boiling, which basically just means they are having rapid density fluctuations and state changes, then the standard deviation will climb. One can also see density reduction in the target by comparing the size of the Lumi signal at different beam currents. One big reason why boiling is such a problem is the formation of small bubbles that effectively causes a fluctuation in the target volume and therefore adds noise to the system, contributing to the overall error of the sample. Ideally one wants to reduce boiling to a negligible contribution.

There are several things that can be done to reduce target boiling, all of which were tried in our studies. One is to change the "raster" size of the beam, which lowers the average current density. This basically just means you can change the area over which the beam is moved from side to side and up and down. In our tests, we used rasters ranging from 1.4mmX1.4mm to 3.8mmX3.8mm to get an idea of exactly what impact the raster has, one can also install a faster raster, which is in the works. The frequency of the fan that cycles the LH2, liquid hydrogen, or LD2, liquid deuterium, from the cooling coils to the target can also by adjusted to try and get better circulation within the target. We tested this characteristic from 10-70 Hz, our adjustable range. Finally, one can just vary the beam current itself. At higher currents, boiling tends to increase, as you might expect. Lowering the current, like decreasing the target length, is self-defeating as it lowers the available luminosity and therefore the figure of merit that has to be achieved. Nevertheless, as a systematic control, we varied the beam current from 0-100 μA. All measures had the anticipated effects, but not

as much as needed to meet our experimental requirements on target noise.

6 Results

In December of 2002 a series of runs were made in Hall A to study cryotarget target boiling effects using the luminosity monitors. Two types of liquid cryogen targets were used. They contained cryogenic hydrogen and deuterium liquids. As a control, a solid carbon target was also installed. The cryotarget cells were of the "beer-can" design and were 4 and 15 cm long. The flow of the liquid in these targets was longitudinal (along the beam axis). In such targets, the longer the target the less uniform the flow, and the more subject the target is expected to be to boiling. One parameter varied was raster size, which effected the local current density of energy deposited to cells.Also varied were the beam current, fan speed of the cryopump, and target length.

It should also be noted that "over sampling" is denoted as OS for the sake of brevity in the plots. For example, OS=13 is a factor of 13 increase in the sampling rate, compared to the actual helicity flip rate of 30Hz.

6.1 Beam Current and Target Length Tests

In figures that plot Lumi σ versus current, one can see the relation between the asymmetry measured by the Lumis and the current of the electron beam. In the 15 cm targets one can see that around a current of 25 μA the Lumi σ stops falling off, as in the case from 0-20 μA, and then rises at higher currents. This is a clear signature of target boiling. In the absence of boiling, we would expect the value of σ to fall off on the order of $1/\sqrt{I}$ because higher current means a greater number of events per unit time. As one can see, the 15 cm LD2 target begins boiling between 20 and 40 μA and the effects of the boiling continue to increase as the current is increased to 100 μA as is shown by the increasing Lumi σ (see Figures 9, 10, 11). In Figure 12 we see an anomaly in that the 4 cm LH2 target does not seem to show signs of boiling until a current of about 40 μA. This is an indication of the more efficient cooling flow in the shorter cells. We can also see that the 15 cm LH2 target boils as much as the LD2 targets. this is because the energy deposit per unit length is about

the same for the two cryogens. This is evident from Figure 13, where we can see the Lumi σ rise rapidly after about 20 μA. Finally, we can see an example of how a non-boiling target behaves using the solid carbon control targets in Figures 14 and 15. In Figure 14, one can see the correspondence of the $1/\sqrt{I}$ with the data points taken from the carbon target. This establishes that the behaviors seen in the other targets are due almost entirely to boiling.

6.2 Fan Speed Tests

In the next 3 figures, the variable we altered was the speed of the cycling fan that keeps the LD2 and LH2 cycling through the targets. Certainly, it is obvious that as the fan speed increases, Lumi σ falls almost linearly(till about 60Hz). The problem, especially in the case of the two 15cm targets, is that even when the fans are at their maximum speed, σ never gets below 6,000 ppm! Ideally, we would like that number to be about an order of magnitude smaller, if we are to observe any significant deviations from the Standard Model in our alloted period of beam time. One nice surprise was the performance of the 4 cm LH2 target. The smaller target seems to have benefitted from better fluid circulation, but, even so, σ never fell below 1300 ppm, which is, at best, about twice what we would like. The 15 cm LD2 target shows an approximately linear dependance on the circulation speed of the target. In Figure 16, the Lumi σ drops from 10,000 ppm at 30 Hz to 6,000 ppm at 70 Hz. The 15 cm LH2 target behaves in much the same way (see Figure 17) only in this case, Lumi σ never gets below about 9,000 ppm which is even worse. Once again the only bright spot is the behavior of the 4 cm LH2 target, which, at 70 Hz, had a σ of about 1,300 ppm (see Figure 18). The sensitivity to target length is an indication that the cell geometry is not optimal, since the energy deposited per unit length is unchanged. In fact, previous experience, with the larger diameter 15 cm long HAPPEX I cells, showed significantly smaller target boiling fluctuations.

6.3 Raster Size Tests

Finally, we tried to adjust the area over which the beam is rastered on the target. The last group of figures show the effect of various raster sizes on target boiling. The general trend, as expected, was for σ to fall as the beam was rastered over a larger area. Obviously,

as the beam energy is dispersed over a larger area, fewer large pockets of boiling emerge. Although we once again got a good showing from the 4cm LH2 target (see Figures 22 and 23), we were still without a single scenario that allowed us to keep σ below 500 ppm(our preferred specification is 480 ppm) while running with a beam current of 100 μA and the long cells needed to meet our experimental specifications on luminosity. Although it might seem reasonable just to run the experiment at 10 μA, it would really be quite impossible. It is hard enough to get an experiment approved for beam time (Even the highest priority experiments often wait years to actually run), but to ask for 10 times the amount of beam time would be absolutely ridiculous.

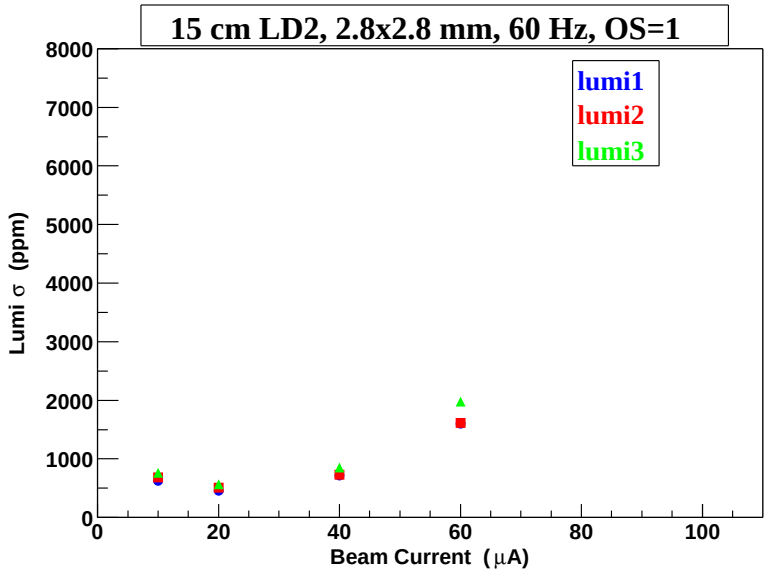

Figure 9: Lumi Sigma vs. Beam Current: Here we can see that increasing the current above 20 μA produces noticeable boiling effects which are measured in terms of the Lumi σ.

7 Summary

Through the testing of the various cryo-targets using lumis, we have been able to determine several things. It has become obvious that when the beam current exceeds 30 μA, boiling compromises the limitations we have placed on error for this experiment. Though the error should decrease like $1/\sqrt{N}$ according to counting statistics, we have found that the error

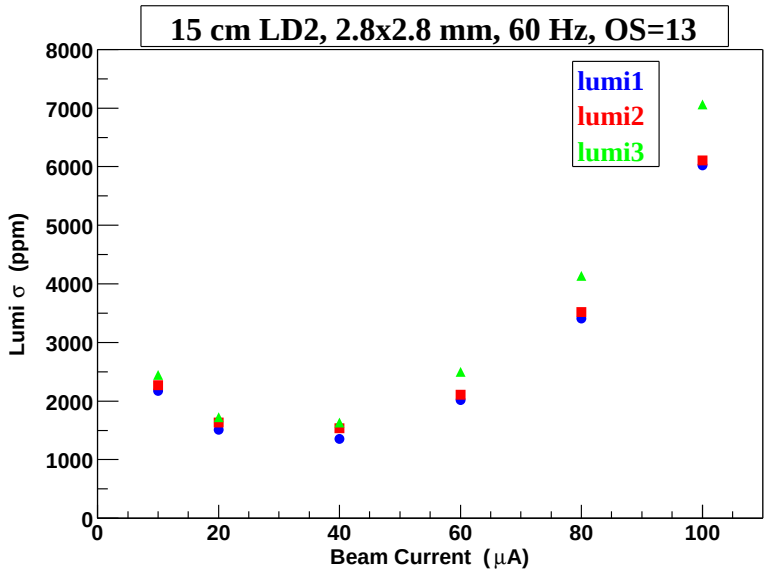

Figure 10: Lumi Sigma vs. Beam Current: This LD2 target shows that at 100 μA, the requisite current for this experiment, the error is on the order of 15 times greater than that which is desired (480 ppm). These effects, which are due to boiling, have the potential to prolong the run time of the experiment, if they are not fixed and/or accounted for.

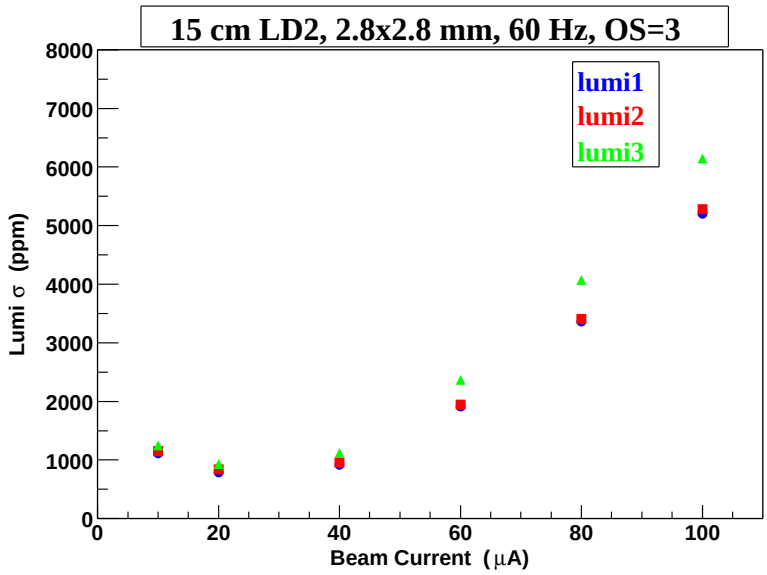

Figure 11: Lumi Sigma vs. Beam Current: As in the previous plots, one can witness that at about 20 μA of beam current, boiling effects begin to emerge and grow increasingly detrimental as the current is raised to 100 μA.

associated with boiling is much higher (relatively) than in HAPPEX I. This is because the statistical error is so much lower. Despite implementing larger raster areas and increasing fan speed, we were unable to find a single target that provided a lumi σ of 480 ppm when the beam current was set at 100 μA.

Despite our best efforts to adjust the fluid flow rate, the raster area of the electron beam, and the spot size of the beam, at currents much above 10 μA, boiling exceeds our design criteria for target related noise in the measurement of the scattering asymmetry. We have, in response to the above findings, concluded that, in order to meet our experimental goals, it is going to be necessary to replace the current targets with a new target design or go back to the targets used in HAPPEX I. This, in fact, is an anticipated result, and plans to built vertical flow "racetrack" cells are well underway. The"race track" targets are the most promising prospect so far . The fluid flow is in the transverse direction in these targets and there are two distinct benefits. First, any boiling which does occur will quickly be swept out of the beam-line to prevent large pockets of gas from developing. Also, the gas will naturally want to rise anyway, so that will increase the speed with which gas pockets clear out as well. Second, there are no areas of longitudinal flow (parallel to the beam-line). In other words,

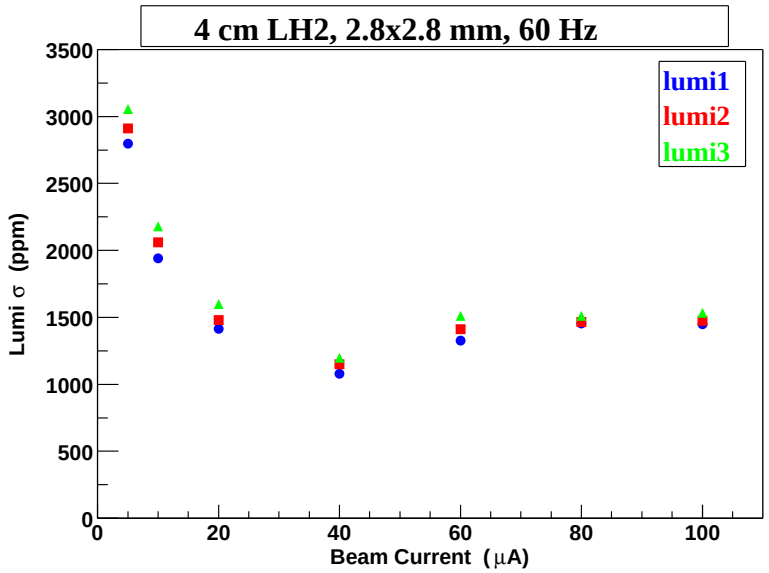

Figure 12: Lumi Sigma vs. Beam Current: This target, 4 cm LH2, shows the most promise of any of our targets so far. Here you can see that boiling effects do not emerge until about 40 μA and after the current is raised to 60 μA the lumi σ levels off. Unfortunately, at 100 μA of current, the error is still a factor of 3 larger than the 480 ppm we would like to see.

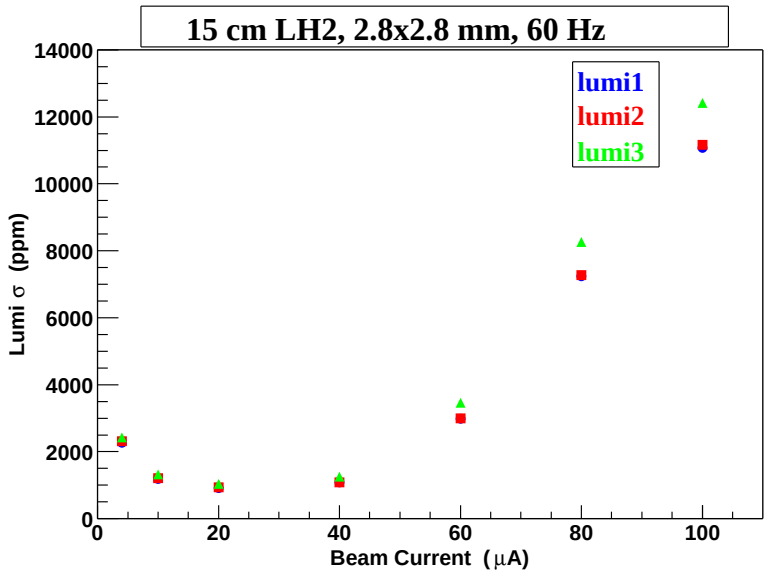

Figure 13: Lumi Sigma vs. Beam Current: The 15 cm LH2 target,unlike its 4 cm counterpart, shows signs of boiling at 20 μA of beam current. At 100 μA, the boiling yeilds a lumi σ of 12,000 ppm!

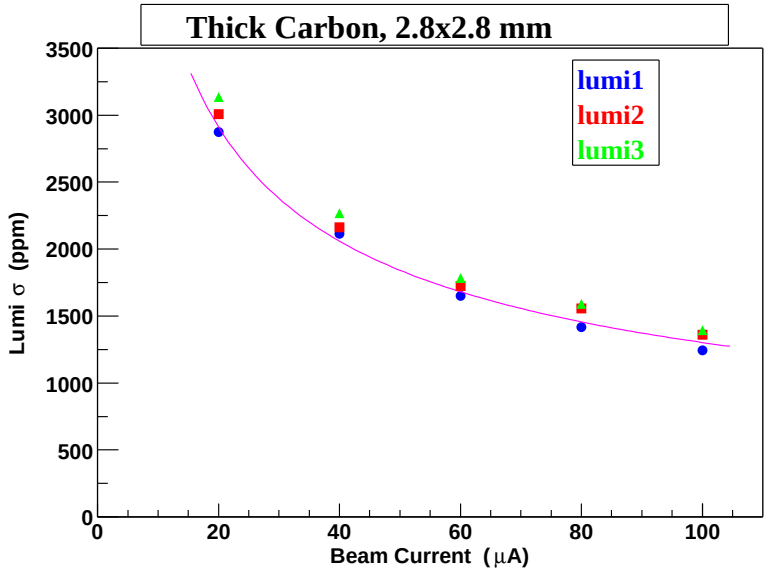

Figure 14: Lumi Sigma vs. Beam Current: Here one can see the dominance of counting statistics in reducing the error of each sampling as current rises in the absence of boiling (solid carbon target). The magenta line is of the form $1/\sqrt{I}$ where I represents the current.

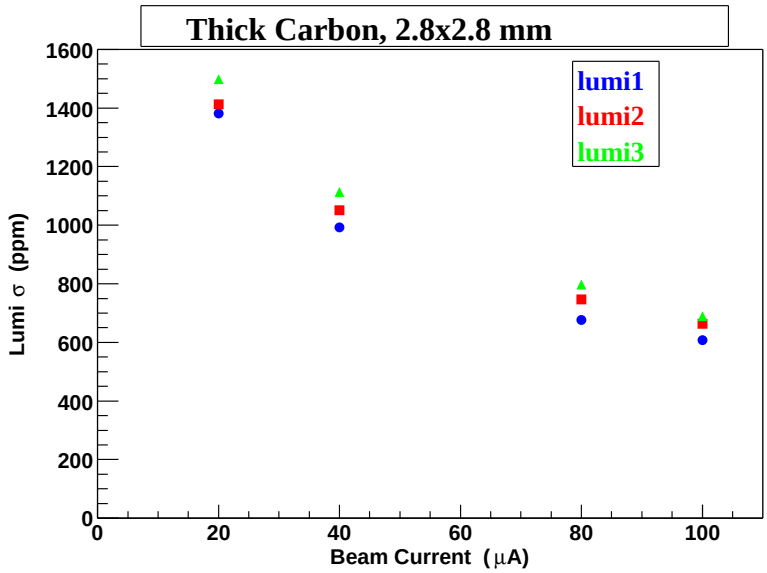

Figure 15: Lumi Sigma vs. Beam Current: This figure is identical to Figure 14 except for the fact that the $1/\sqrt{I}$ line is not drawn.

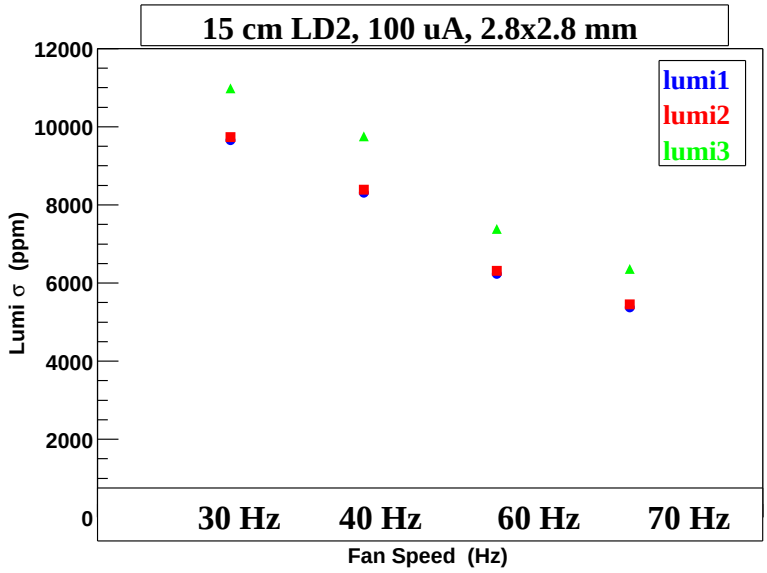

Figure 16: Lumi Sigma vs. Fan Speed: Here one can see the effect of circulating LD2 through the target at a higher rate. As the circulating fan's speed is increased from 30 Hz to 70 Hz, σ is cut in half, but still remains a factor of 10 above what is required (480 ppm).

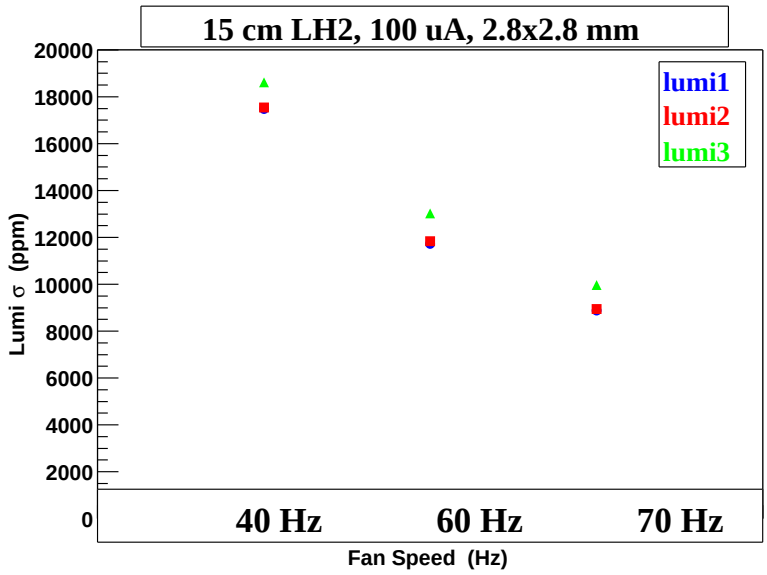

Figure 17: Lumi Sigma vs. Fan Speed: This 15 cm LH2 target displays a nearly linear dependance of σ on fan speed. Again, the boiling effects, as can be seen by value of lumi σ, keep the error of the sample at a level far above what is needed.

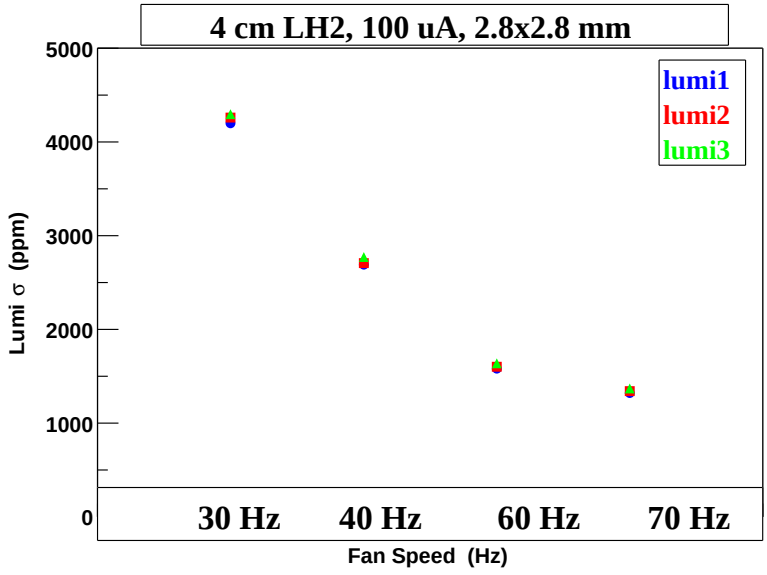

Figure 18: Lumi Sigma vs. Fan Speed: Once again, the LH2 target performs much better than the 15 cm targets, but with a value of only 1,500 ppm for lumi σ at a fan speed of 70 Hz, this target performs a factor of 3 worse than the experimental specifications.

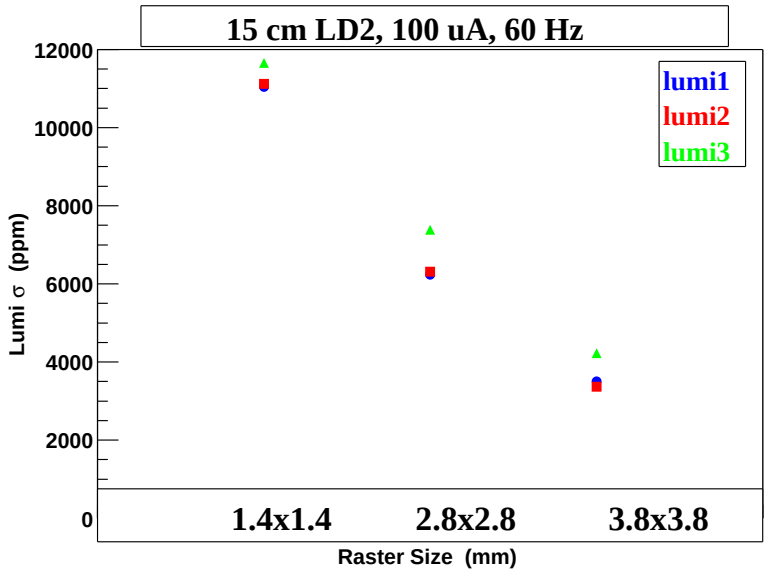

Figure 19: Lumi Sigma vs. Raster size: This figure shows that boiling is clearly reduced when the area over which the beam-line is rastered is increased. This can be seen by observing the falling values of σ as raster size increases from a 1.4x1.4 mm square to one that is 3.8x3.8 mm.

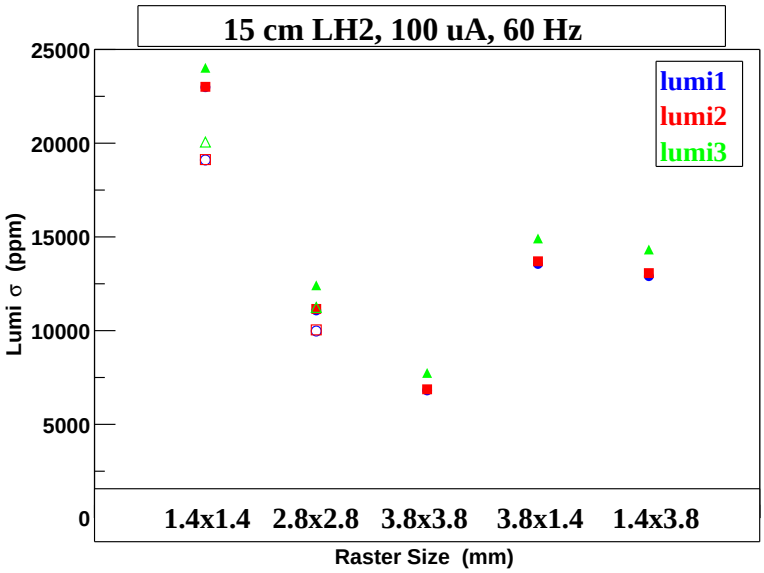

Figure 20: Lumi Sigma vs. Raster size: This 15 cm LH2 target shows that increasing the area over which the beam-line is rastered (fancy word for "moved"), decreases the effects of boiling but, once again, the error is still far too high.

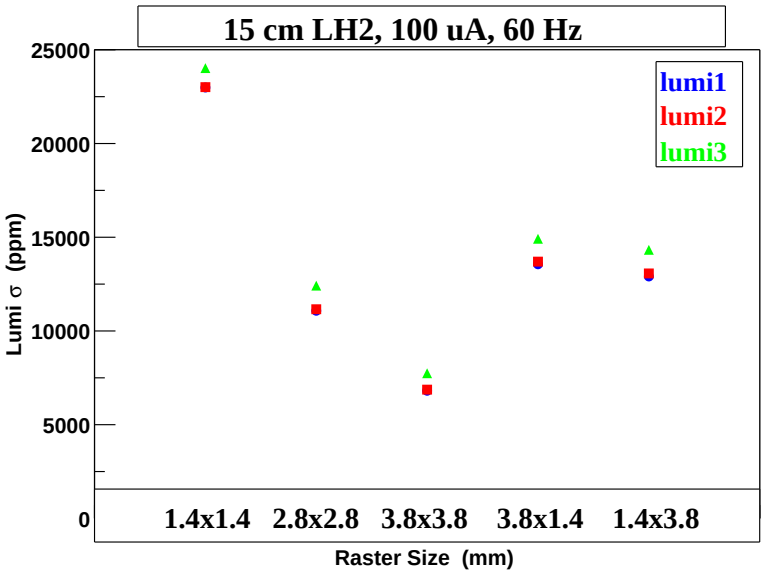

Figure 21: Lumi Sigma vs. Raster size: This plot shows that a larger rastering area decreases the effects of boiling.

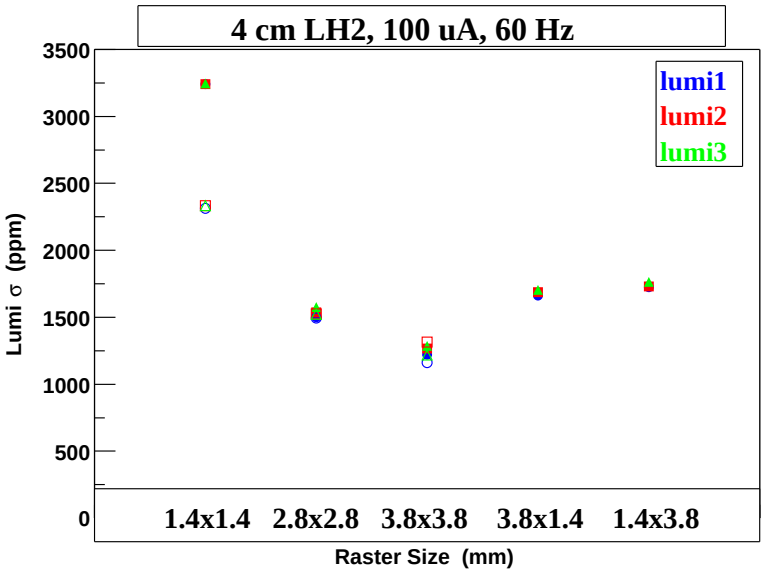

Figure 22: Lumi Sigma vs. Raster size: Though this plot has the same appearance as Figures 20 and 21, it is important to note the scale. This target has a σ a factor of 5 smaller. This target has once again performed better than the 15 cm targets.

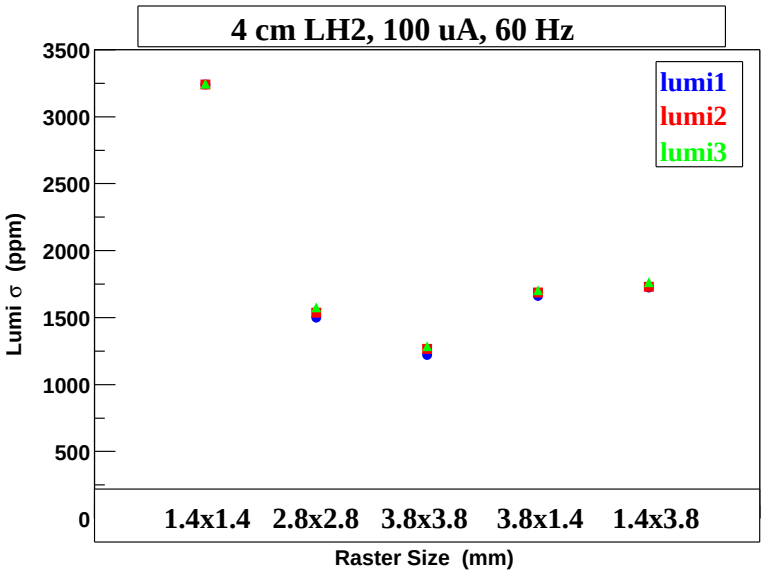

Figure 23: Lumi Sigma vs. Raster Size: At a rastering area of 3.8 x 3.8 mm, one can see the lumi σ fall to approximately 1,200 ppm.

because the flow is constant through the window where the electron beam enters the fluid, the fluid does not get heated on its way to the window. Certainly it is essential that these new targets get the same rigorous testing as their "beer can" counterparts, but the outlook is good.

Another possibility that we must consider is that if we must use "beer can" targets, we might be able to account for the boiling deviations by sampling at a higher frequency. In Figure 24 one can see the fluctuations due to boiling occur on the time scale of around 50-100 ms. It is possible that if we sampled at a much higher frequency, then we could measure and subtract the error attributed to boiling and perhaps manage to get lumi σ below 480 ppm ([8]).

In a very recent reanalysis [8] of our data, the oversampling of the data was examined. Figure 24 show the time structure of the ^{12}C and 15 cm LD2 targets at 60 μA for an oversampling factor of 13 . The top figure for carbon is highly expanded and shows expected random statistical behavior. For the lower figure, the width of the curve is due to the statistical error, while the rapid swings with a 50-100 ms time structure are due to bubble formation and collapse and/ or removal. This is an exciting result, since it indicates that by normalizing our signal to the luminosity monitors, we can effectively remove a major part of the boiling noise. Obviously, we hope to have our cake and eat it too by building targets with small noise, and then verifying and correcting for any residual effect.

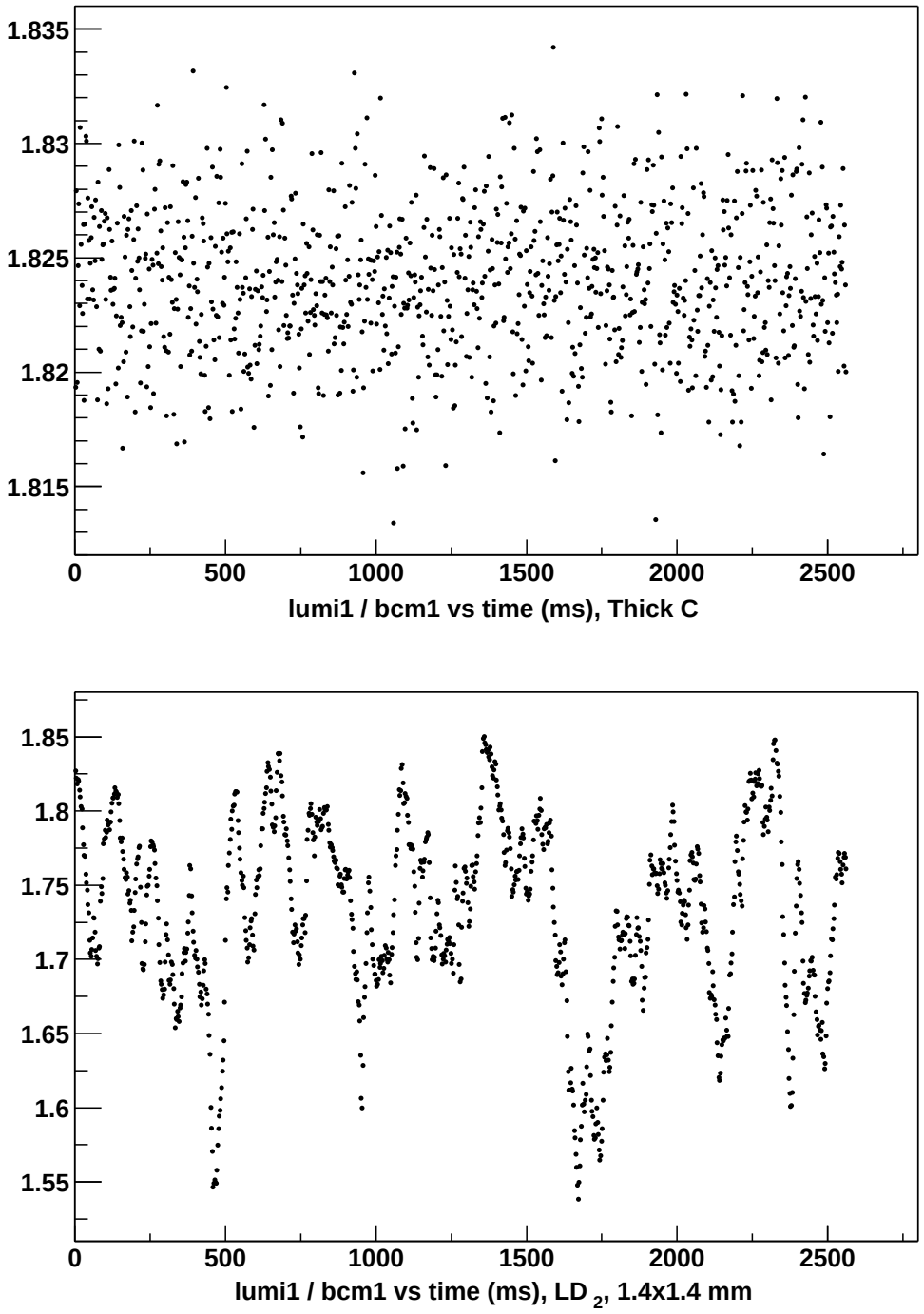

Figure 24: Carbon versus LD2: This figure shows how the relation between lumi1 and bcm1 varies between the carbon target and the LD2 target. What you see here is that in the absence of boiling, bcm1 and lumi1 agree. In the case of LD2 however, you can see each specific instance of boiling in the spikes on the plot.

8 Aknowledgements

I must sincerely express my gratitude at the privilege of having worked with two most brilliant and helpful men. Prof. Mike Finn (W&M) and Riad Suleiman (MIT) were not just great people to get to know, but they also helped me immensely in undertaking this project. They helped to answer my many questions and showed me patience, even though I am sure it was quite difficult at times. I wish them both the best and hope that they can have the impact on many more that they had on me. I would also like to thank all those at Jefferson Lab that I had the priveledge of working with. From Mary, the kind lady in dining services, to Bob, a friend from the JLAB basketball team, I'd like to thank everyone for making my research more enjoyable.

References

[1] C. S. Wu *et al.*, Phys. Rev. **105**, 1413 (1957).

[2] K. Aniol *et al.*, Phys. Rev. Lett. **82**, 1096 (1999).

[3] W. Miller, Ph.D. thesis, Princeton University, 2001 (unpublished).

[4] JLab Proposal E-99-115, K. Kumar and D. Lhuillier, spokespersons (1999).

[5] JLab Proposal E-00-114, D. Armstrong and R. Michaels, spokespersons (2000).

[6] JLab Proposal E-91-017, D. H. Beck, spokesperson (1991).

[7] B. Mueller *et al.*, Phys. Rev. Lett. **78**, 3824 (1997).

[8] D.S. Armstrong *et al.*, Target Density Fluctuations and Bulk Boiling in the Hall A Cryotarget, 2003.

[9] G. Rutledge, Measurement of the Strange Sea of the Proton (2001)